引用格式：HAN Jinzhuang, LI Xinqiang, SHEN Jin, et al. Regularization Inversion with Preconditioner for Flowing Aerosols in Dynamic Light Scattering[J]. Acta Photonica Sinica, 2022, 51(11):1101002
韩锦壮,李鑫强,申晋,等.结合条件预优的流动气溶胶动态光散射正则化反演[J].光子学报,2022,51(11):1101002

结合条件预优的流动气溶胶动态光散射正则化反演

韩锦壮,李鑫强,申晋,王保珺,刘伟,王雅静
(山东理工大学 电气与电子工程学院,山东 淄博 255049)

摘　要:为提高流动气溶胶动态光散射粒度反演的准确性,采用结合条件预优的流动气溶胶正则化反演,通过条件预优处理,以先验流速信息和延迟时间构建对角阵形式的条件预优矩阵,对病态方程实现乘法修正,从而降低了流速对反演方程病态性的加剧作用和正则化方法对流速的敏感性。模拟与实测数据的反演结果表明,与 Tikhonov 正则化反演相比,结合条件预优的 Tikhonov 正则化反演,可克服正则化在流动颗粒粒度反演中的局限性,显著改善了流动气溶胶动态光散射测量数据的反演性能指标,提高了正则化反演结果的准确性。

关键词:动态光散射;气溶胶;反演;颗粒测量;正则化;条件预优
中图分类号:O439　　**文献标识码**:A　　**doi**:10.3788/gzxb20225111.1101002

0　引言

动态光散射(Dynamic Light Scattering, DLS)技术是测量亚微米及纳米颗粒粒度及其分布的有效方法[1],该方法通过测量悬浮颗粒散射光强信号的自相关函数(Autocorrelation Function, ACF),来获取颗粒的粒度分布(Particle Size Distribution, PSD)信息[2-4]。常规的DLS测量是针对非流动样品在固定容器中进行,样品中除布朗运动外的其它宏观运动被认为是不存在的。与稳态悬浮颗粒的DLS测量不同,对于流动颗粒,由于附加平移运动导致的对传统DLS理论的修正,在理论与实践中都极大地增加了动态光散射测量的难度。

对流动颗粒进行DLS测量的探索可追溯到20世纪80年代,CHOWDHURY D P等[5]推导了单分散流动颗粒的ACF模型,将原表征布朗运动的扩散项改为其与表征定向运动的平移项的乘积。1986年,TAYLOR T W和SORENSEN C M[6]通过研究入射光束的高斯形状特征,发现平移项所对应的平移特征时间是由流速和入射光束交点处的束腰半径所决定,与散射体相较在入射光束焦点的位置无关,他们因此将ACF表达式中的高斯光束半径改为高斯光束焦点处的束腰半径。1998年,WEBER R等建立了多分散流动颗粒的ACF理论模型[7],进而提出可通过拟合ACF获取气溶胶的颗粒粒度、浓度和流速[8]。此后,用于自混频相干测量的流动布朗运动颗粒的ACF和功率谱模型也建立起来[9]。2021年,牟彤彤等基于WEBER R的ACF模型进行了流动气溶胶PSD的实测[10],进而分析了流动对气溶胶PSD测量的制约机制[11]:流动气溶胶粒度反演困难的一个重要原因是,流速的增加导致ACF反演方程的病态性加剧,表现为反演方程核矩阵条件数增大。

正则化方法是改善病态方程核矩阵条件数的常用方法,其基本原理是通过对核矩阵的奇异值进行加法修正来实现核矩阵条件数的降低[12-13],已在常规DLS粒度反演中得到广泛应用。对于流动颗粒,反演方程

基金项目:山东省自然科学基金(No. ZR2020MF124),淄博市重点研发计划(校城融合发展类)(No. 2019ZBXC011)
第一作者:韩锦壮(1995—),男,硕士研究生,主要研究方向为动态光散射测量。Email: 17865918325@163.com
导师(通讯作者):申晋(1962—),男,教授,博士,主要研究方向为光电精密测试技术。Email: shenjin@sdut.edu.cn
收稿日期:2022-05-12;**录用日期**:2022-06-15

的病态程度随着流速的增加而显著增大，反演过程中正则化方法对病态程度的降低受到流速增加的制约。为在较高流速下得到更为准确的PSD，本文采用条件预优[14-15]结合Tikhonov正则化方法进行流动气溶胶的PSD反演，通过条件预优利用先验流速信息降低核矩阵条件数，显著改善了颗粒流动引起反演方程病态性增高导致的PSD准确性降低的问题。

1 流动气溶胶DLS测量原理

散射场中，光强ACF与电场ACF满足Siegert关系[16]

$$g^{(2)}(\tau)=1+\beta\left|g^{(1)}(\tau)\right|^2 \tag{1}$$

式中，$g^{(2)}(\tau)$为归一化的光强ACF，τ为延迟时间，β为相干因子，$g^{(1)}(\tau)$为归一化电场ACF。

对于单分散颗粒系，电场ACF为指数衰减函数

$$g^{(1)}(\tau)=\exp(-\Gamma\tau) \tag{2}$$

式中，Γ为衰减线宽，其表达式为

$$\Gamma=\frac{16\pi k_{\mathrm{B}}Tn^2}{3\eta d{\lambda_0}^2}\sin^2\left(\frac{\theta}{2}\right) \tag{3}$$

式中，d为颗粒粒度大小，k_{B}、T、η、λ_0、n和θ分别为玻尔兹曼常数、绝对温度、介质的粘滞系数、入射光波长、介质的折射率和散射角度。

对于流动颗粒，光强ACF衰减由扩散运动与平移运动两部分共同作用，若散射体内的颗粒数足够多，则其电场ACF为[10]

$$g^{(1)}(\tau)=\exp(-\Gamma\tau)\exp\left(-\frac{v^2}{2\omega^2}\tau^2\right) \tag{4}$$

式中，v为气溶胶颗粒流速，$\omega=\dfrac{\lambda_0}{\pi\omega_0}f_1$为聚焦束腰，$\omega_0$为入射光的束腰，$f_1$为透镜的焦距。对于多分散气溶胶，以衰减线宽为权重来表示$g^{(1)}(\tau)$，其离散化形式为

$$g^{(1)}(\tau)=\sum_{i=1}^{N}G(\Gamma_i)\exp(-\Gamma_i\tau)\exp\left(-\frac{v^2}{2\omega^2}\right) \tag{5}$$

式中，N为离散的颗粒点数，$G(\Gamma_i)$为归一化的衰减线宽分布，满足$\sum_{i=1}^{N}G(\Gamma_i)=1$。将式(3)带入式(5)，并直接以颗粒粒度为权重表示电场ACF，可以得到

$$g^{(1)}(\tau)=\sum_{i=1}^{N}\exp\left[-\frac{16\pi k_{\mathrm{B}}Tn^2}{3\eta d_i{\lambda_0}^2}\sin^2\left(\frac{\theta}{2}\right)\tau\right]\exp\left(-\frac{v^2}{2\omega^2}\tau^2\right)f(d_i) \tag{6}$$

式中，$f(d_i)$为离散PSD，满足$\sum_{i=1}^{N}f(d_i)=1$。式(6)的向量形式为

$$\boldsymbol{g}=\boldsymbol{A}\boldsymbol{f} \tag{7}$$

式中，$\boldsymbol{g}$是由$g^{(1)}(\tau_j)$组成的列向量，$j=1,2,\cdots,M$，M为延迟通道数，$\boldsymbol{f}$是由$f(d_i)$组成的列向量，$i=1,2,\cdots,N$，核矩阵$\boldsymbol{A}$可表示为

$$\boldsymbol{A}_{(j,i)}=\exp\left[-\frac{16\pi n^2k_{\mathrm{B}}T}{3\eta{\lambda_0}^2d_i}\sin^2\left(\frac{\theta}{2}\right)\tau_j\right]\exp\left(-\frac{v^2}{2\omega^2}{\tau_j}^2\right) \tag{8}$$

式(7)为一典型的病态方程，$\boldsymbol{g}$的微小改变便会引起解的巨大变化。Tikhonov正则化通过正则参数和正则矩阵作用于原病态核矩阵来改善方程的病态性，其表达式为

$$J_\alpha(\boldsymbol{f})=\min\left\{\left\|\boldsymbol{A}\boldsymbol{f}-\boldsymbol{g}\right\|_2^2+\alpha^2\left\|\boldsymbol{L}\boldsymbol{f}\right\|_2^2\right\} \tag{9}$$

式中，$\|\cdot\|_2$为欧式范数，α为正则参数，采用L-curve准则选取，起到平衡病态核矩阵与正则化矩阵的作用，反映了正则化矩阵的权重大小。$\boldsymbol{L}$为正则矩阵，选用二阶差分矩阵，起到修正病态核矩阵的作用。$\boldsymbol{f}$为颗粒粒度分布，需要添加非负约束。式(9)的等价形式可转化为

$$J_a(\boldsymbol{f})=\left\|\begin{bmatrix}\boldsymbol{A}\\ \alpha\boldsymbol{L}\end{bmatrix}\boldsymbol{f}-\begin{bmatrix}\boldsymbol{g}\\ 0\end{bmatrix}\right\|_2^2 \qquad s.t.0\leqslant f(d)\leqslant 1 \tag{10}$$

不同于非流动悬浮颗粒粒度分布的常规DLS反演，由于流动气溶胶存在定向运动，其光强ACF为表征布朗运动的扩散项与表征定向运动的平移项间的乘积，导致反演方程的病态性增加。设核矩阵$\boldsymbol{A}$中相应参数为分别为：λ_0=532 nm，T=298.15 K，n=1.000 3，θ=90°，k_B=1.380 7×10^{-23} J·K^{-1}，η=18.37×10^{-3} mPa·s，入射光束腰ω_0=0.409 mm，透镜焦距f_1=175 mm。光强ACF的延迟时间为1 μs到4 000 μs，按比例间隔分25组，每组内延迟时间按线性间隔。反演的PSD取值按8.32 nm间隔，在2.01 nm到1 000.01 nm之间取120个点。可计算出流速为0 m/s、0.4 m/s、0.8 m/s、1.2 m/s、1.6 m/s和2.0 m/s时的条件数分别为3.63×10^{19}、3.93×10^{22}、4.08×10^{31}、3.38×10^{48}、1.15×10^{70}和8.07×10^{97}，可见，流速的增加导致病态性的显著增大。采用Tikhonov正则化后，方程的条件数分别降低为3.04×10^7、3.94×10^7、4.04×10^7、4.91×10^7、5.87×10^{7}和7.86×10^7，可以看出，相对于原方程，正则化方法可显著降低条件数。但是，流动条件下的条件数明显高于非流动情况，随着颗粒流速的增加正则化方法的条件数也随之增加，直接的后果是，流速的增加导致反演结果失真。

为降低流速增加对反演结果的影响，本文对反演方程进行条件预优化处理，即，构造与式(7)等价的方程组

$$\boldsymbol{Pg}=\boldsymbol{PAf} \tag{11}$$

式中，$\boldsymbol{P}>0$，为条件预优矩阵，满足

$$\mathrm{cond}(\boldsymbol{PA})\leqslant\mathrm{cond}(\boldsymbol{A}) \tag{12}$$

可利用先验流速信息和延迟时间构造为$M\times M$维方阵

$$\boldsymbol{P}=\begin{bmatrix}\exp\left(\frac{v^2}{2\omega^2}\tau_1\right) & 0 & \cdots & 0\\ 0 & \exp\left(\frac{v^2}{2\omega^2}\tau_2\right) & \cdots & 0\\ \vdots & \vdots & \ddots & \vdots\\ 0 & 0 & \cdots & \exp\left(\frac{v^2}{2\omega^2}\tau_M\right)\end{bmatrix} \tag{13}$$

将式(13)带入式(11)

$$\exp\left(\frac{v^2}{2\omega^2}\tau\right)\cdot g^{(1)}(\tau)=\sum_{i=1}^{N}\exp\left[-\frac{16\pi n^2 k_B T}{3\eta\lambda_0{}^2 x_i}\sin^2\left(\frac{\theta}{2}\right)\tau\right]f(d_i) \tag{14}$$

得条件预优结合Tikhonov正则化方法求取$f(d_i)$的表达式

$$J_a(\boldsymbol{f})=\left\|\begin{bmatrix}\boldsymbol{PA}\\ \alpha\boldsymbol{L}\end{bmatrix}\boldsymbol{f}-\begin{bmatrix}\boldsymbol{Pg}\\ 0\end{bmatrix}\right\|_2^2 \qquad s.t.0\leqslant f(d_i)\leqslant 1 \tag{15}$$

不难看出，经过条件预优处理后的核矩阵条件数不再受流速的影响。

2 模拟数据反演

模拟的多分散气溶胶PSD采用正态分布[17]

$$f(d)=\frac{a}{\sqrt{2\pi}\,\sigma_1}\exp\left(-\frac{(d-\mu_1)^2}{2\sigma_1{}^2}\right)+\frac{b}{\sqrt{2\pi}\,\sigma_2}\exp\left(-\frac{(d-\mu_2)^2}{2\sigma_2{}^2}\right) \tag{16}$$

式中，a和b为PSD峰值权重的比例参数，且满足$a+b=1$，μ_1和μ_2为PSD峰值对应的粒度，σ_1和σ_2为颗粒粒度分布的标准差。表1为模拟PSD的分布参数，模拟时通过分段积分对连续分布离散化。模拟实验条件为λ_0=532 nm，ω_0=0.409 mm，f_1=175 mm，T=298.15 K，n=1.000 3，θ=90°，k_B=1.380 7×10^{-23} J·K^{-1}，η=18.37×10^{-3} mPa·s，β=0.7。模拟中对应光强ACF的延迟时间按1 μs到4 000 μs分25组，取150个值，分组

按组间比例间隔、组内线性间隔。单峰粒度范围从208 nm到1 000 nm，双峰粒度范围从8 nm到1 000 nm，颗粒粒度间隔均为4 nm。

表1 模拟PSD的参数

Table 1 PSD simulation parameters

Peak/nm	a	b	μ_1	σ_1	μ_2	σ_2
600	1	0	600	30	—	—
200/700	0.5	0.5	200	30	700	30

为与实测情况吻合，模拟中数据加入高斯随机噪声

$$g^{(2)}{}_{\text{noise}}(\tau)=g^{(2)}(\tau)+0.001n(\tau) \tag{17}$$

式中，$n(\tau)$为高斯随机噪声。

流速取值范围通过雷诺数限制，以保证流体处于层流状态。雷诺数为

$$Re=\rho_0 D_0 v/\eta \tag{18}$$

式中，ρ_0和D_0分别为流体介质的密度和流体所经圆管的当量直径。取$\rho_0=1.293\ \text{kg/m}^3$，$D_0=12$ mm，由层流条件下雷诺数范围($Re\leqslant 2\,000$)得气溶胶流速范围为0～2.3 m/s。以0.4 m/s为间隔，从0.4 m/s到2.0 m/s选取5个速度值作为已知条件参数。

粒度反演时，根据式(1)由光强ACF求得电场ACF，再通过电场ACF反演颗粒粒度。反演效果通过峰值位置相对误差E_P和分布误差E_F评估

$$E_P=\frac{|P_{\text{true}}-P_{\text{measure}}|}{P_{\text{true}}} \tag{19}$$

$$E_F=\left\{\left(\sum_1^K[f_{\text{true}}(d)-f_{\text{measure}}(d)]^2\right)/N\right\}^{1/2} \tag{20}$$

式中，P表示峰值位置处的粒径，下标true和measure分别表示真实值和反演值。

图1和图2分别为600 nm单峰分布和200 nm/700 nm双峰分布气溶胶颗粒在不同流速下的反演结果，相应的性能参数如表2和表3所示。图中的“true PSD”表示真实的粒度分布，“Tik”代表Tikhonov正则化，“Pre-Tik”代表结合条件预优的Tikhonov正则化，表中的PP表示峰值位置，Cond表示反演方程核矩阵的条件数。

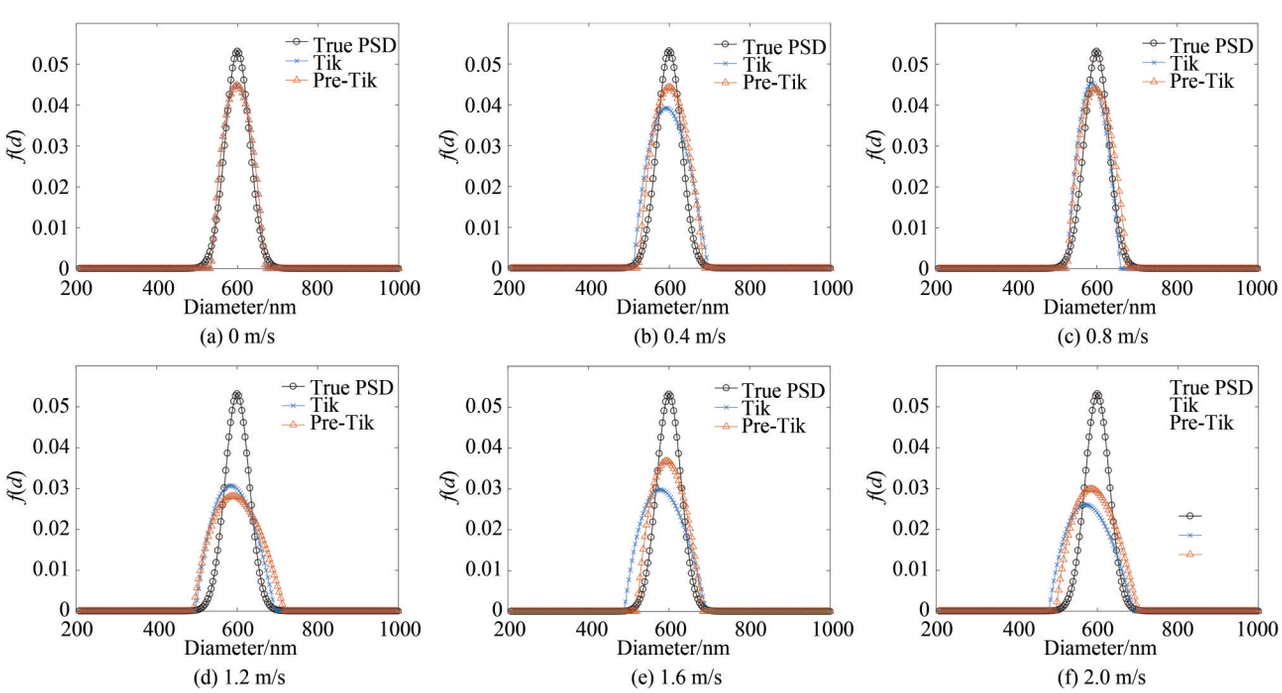

图1 600 nm单峰气溶胶不同速度下的反演结果

Fig. 1 The recovery of 600 nm unimodal aerosol PSDs at different velocities

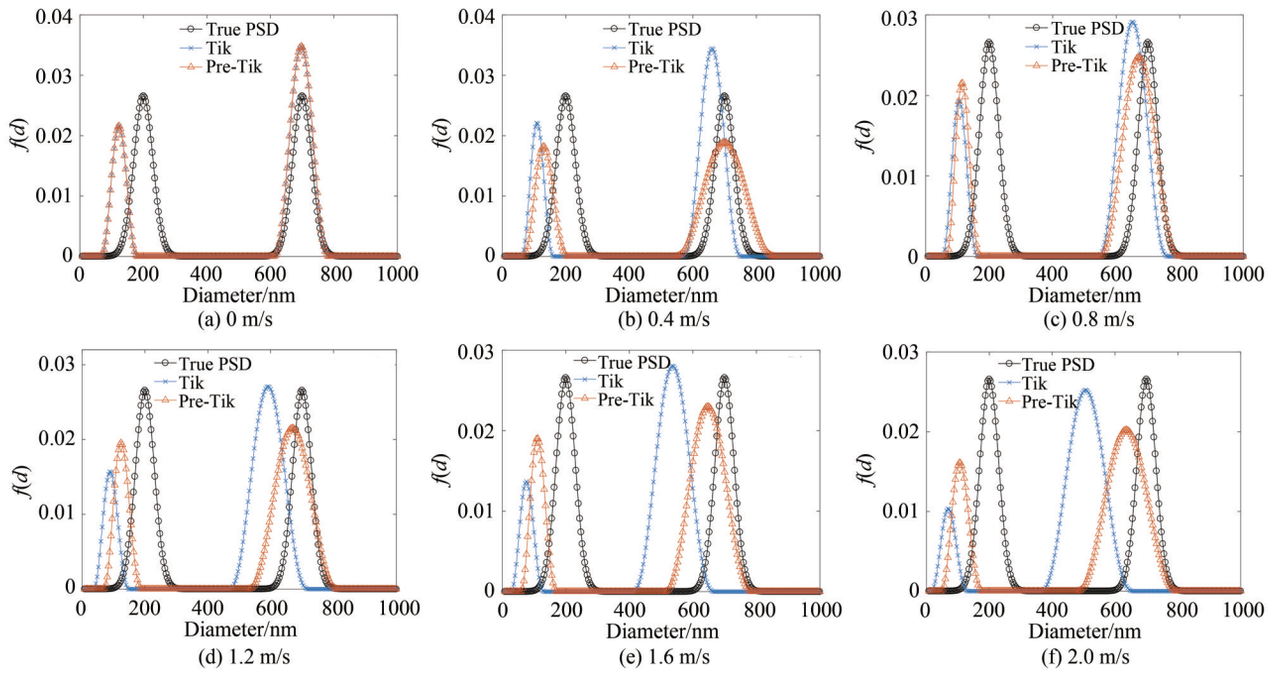

图 2　200 nm/700 nm 双峰气溶胶不同速度下的反演结果

Fig.2　The recovery of 200 nm/700 nm bimodal aerosol PSDs at different velocities

表 2　600 nm 单峰气溶胶反演结果的性能指标

Table 2　The performance indices of the recovery of 600 nm unimodal PSDs

Velocity/(m•s^{-1})	Method	PP/nm	E_P	E_F	Cond
0	Tik	600	0	0.002 0	3.86×10^{8}
	Pre-Tik	600	0	0.002 0	3.86×10^{8}
0.4	Tik	592	0.013 3	0.004 7	7.07×10^{8}
	Pre-Tik	600	0	0.003 7	3.86×10^{8}
0.8	Tik	588	0.020 0	0.003 2	8.68×10^{8}
	Pre-Tik	596	0.006 7	0.002 9	3.86×10^{8}
1.2	Tik	584	0.026 7	0.005 6	1.24×10^{9}
	Pre-Tik	588	0.020 0	0.006 1	3.86×10^{8}
1.6	Tik	576	0.040 0	0.006 1	1.35×10^{9}
	Pre-Tik	592	0.013 3	0.003 7	3.86×10^{8}
2.0	Tik	572	0.046 7	0.006 9	1.51×10^{9}
	Pre-Tik	584	0.026 7	0.005 7	3.86×10^{8}

从图 1 和表 2 可以看出,对于 600 nm 单峰气溶胶,随着流速的增加,反演结果中 PSD 出现展宽,峰值位置左移,Tik 方法的 E_P 和 E_F 分别由 0 和 0.002 0 增大到 0.046 7 和 0.006 9。在流速相同的条件下,Pre-Tik 方法的反演结果优于 Tik 方法,并且随着流速的增大,Pre-Tik 方法的优化效果愈趋明显。颗粒流速为 0 时,两种方法的 E_P 和 E_F 相同,当流速达 2.0 m/s 时,Pre-Tik 方法得到的 E_P 和 E_F 分别降低到 0.026 7 和 0.005 7。

从图 2 和表 3 可以看出,在 200 nm/700 nm 双峰气溶胶反演结果中,两个峰均向粒度减小的方向偏移,且偏移随流速增加逐渐增大,峰值位置误差和分布误差随之增大,但两种方法反演结果的性能指标差异显著,当流速为 2 m/s 时,Tik 方法反演结果的 E_P 和 E_F 分别为 0.660 0/0.274 3 和 0.012 1,Pre-Tik 方法的 E_P 和 E_F 则分别为 0.460 0/0.091 4 和 0.009 1,反演结果的准确性显著提高。

表 3 200 nm/700 nm 双峰气溶胶反演结果的性能指标

Table 3 The performance indices of the recovery of 200 nm/700 nm bimodal PSDs

Velocity/(m·s^{-1})	Method	PP/nm	E_P	E_F	Cond
0	Tik	124/696	0.380 0/0.005 7	0.007 6	4.40×10^{8}
	Pre-Tik	124/696	0.380 0/0.005 7	0.007 6	4.40×10^{8}
0.4	Tik	108/660	0.460 0/0.057 1	0.009 7	7.99×10^{8}
	Pre-Tik	132/700	0.340 0/0	0.007 2	4.40×10^{8}
0.8	Tik	104/652	0.480 0/0.068 6	0.009 6	1.22×10^{9}
	Pre-Tik	116/672	0.420 0/0.040 0	0.008 3	4.40×10^{8}
1.2	Tik	88/592	0.560 0/0.154 3	0.011 7	1.55×10^{9}
	Pre-Tik	124/668	0.380 0/0.045 7	0.008 0	4.40×10^{8}
1.6	Tik	76/536	0.620 0/0.234 3	0.012 4	1.76×10^{9}
	Pre-Tik	112/648	0.440 0/0.074 3	0.009 1	4.40×10^{8}
2.0	Tik	68/508	0.660 0/0.274 3	0.012 1	1.90×10^{9}
	Pre-Tik	108/636	0.460 0/0.091 4	0.009 1	4.40×10^{8}

3 实验

实验数据取自本课题组研制的流动气溶胶DLS在线测量实验平台(图3(a)),实验装置主要由气溶胶发生器、导管、比色皿、激光、光子计数探测器、光子相关器等组成。单、双峰分布气溶胶分别由3321PLUS和SX-Q5气溶胶发生器产生,激光器采用MGL-III-532nm-10mW,光子计数探测器选用CH326、光子相关器选用Brookhaven BI-9000AT(图3(b)),流速通过热线风速仪SAR886A测量,其他实验参数与模拟参数相同。相关器取150个延迟通道,通道从1μs到4000μs分25组,组间比例间隔、组内线性间隔。颗粒粒度以10 nm间隔从10 nm到1 000 nm取100个点。粒度反演时,通过来自光子相关器的光强ACF,计算出电场ACF,再由电场ACF反演PSD。反演结果如图4、图5、图6和表4、表5所示,反演结果的峰值位置误差和分布误差分别用E_{P0}和E_{F0}表示,0 m/s时的反演结果作为对比参照的气溶胶分布。

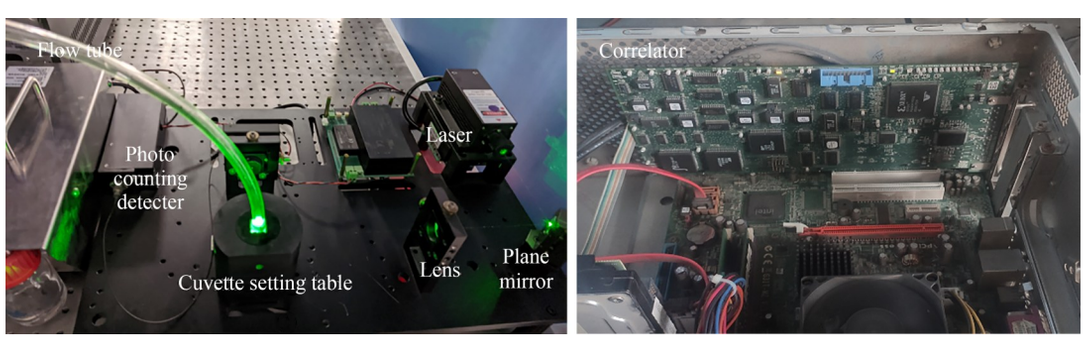

图 3 实验装置和相关器

Fig. 3 Experimental devices and Correlator

从图5和表4可以看出,对于单峰气溶胶,在流速为1.09 m/s和1.77 m/s时,Tik方法反演结果的E_{P0}分别为0.052 6和0.087 7,E_{F0}分别为0.006 3和0.019 0,Pre-Tik方法得到的E_{P0}分别为0.035 1和0.052 6,E_{F0}分别为0.004 5和0.016 2,后一方法反演效果好于前者。

图6和表5表明,双峰气溶胶的正则化反演对流速表现得更为敏感,与Tik方法相比,Pre-Tik方法反演的峰值位置误差和分布误差均显著下降。当速度为1.28 m/s时,Tik方法反演出的小峰峰高仅为0速对应PSD小峰峰高的0.092 6倍,而Pre-Tik方法反演出的小峰峰高为0速对应PSD峰高的0.247 2倍,Pre-Tik方法反演结果的大峰峰值位置误差约为Tik方法的1/3,Pre-Tik方法的小峰峰值位置误差仅为Tik方法的1/5,改善效果显著。

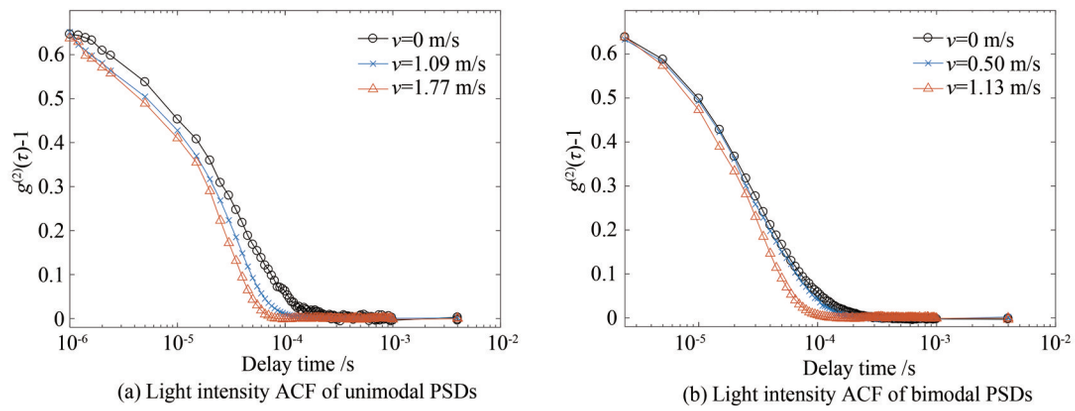

图 4　不同流速下气溶胶颗粒的光强 ACF

Fig. 4　Measured light intensity ACFs at different velocities

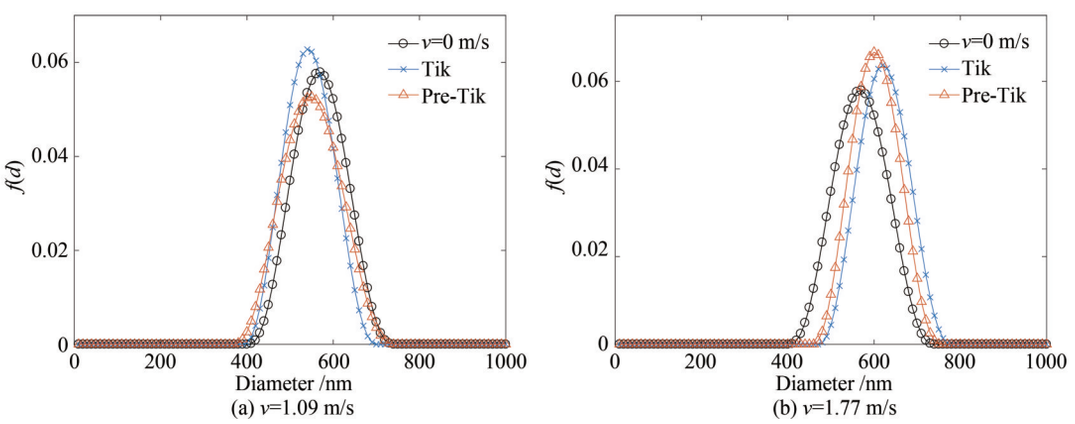

图 5　不同流速时单峰气溶胶的反演结果

Fig. 5　The recovery of unimodal aerosol PSDs at different velocities

表 4　单峰气溶胶反演结果的性能指标

Table 4　The performance indices of the recovery of unimodal PSDs

Velocity/(m•s^{-1})	Method	PP/nm	E_{P0}	E_{F0}	Cond
0	Tik	570	0	0	2.41×10^{7}
1.09	Tik	540	0.052 6	0.006 3	5.52×10^{7}
	Pre-Tik	550	0.035 1	0.004 5	2.41×10^{7}
1.77	Tik	620	0.087 7	0.012 4	8.07×10^{7}
	Pre-Tik	600	0.052 6	0.008 6	2.41×10^{7}

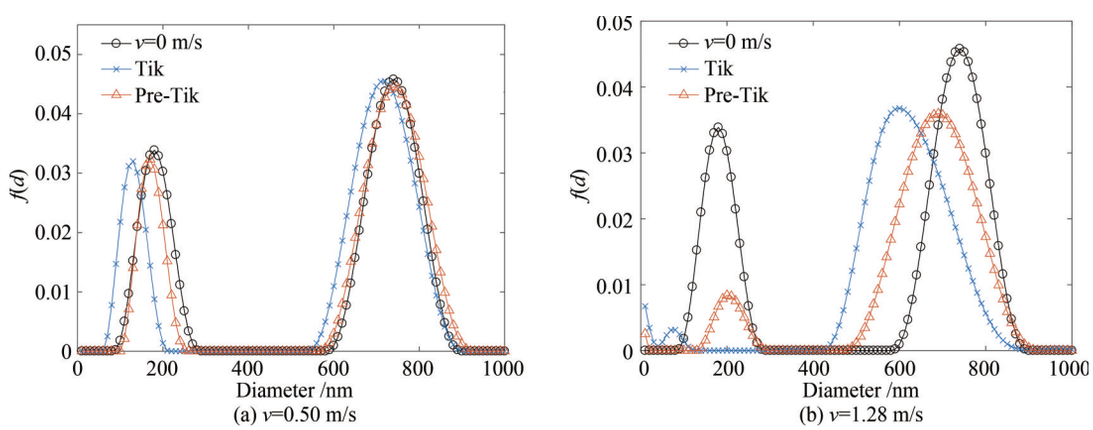

图 6　不同流速时双峰气溶胶的反演结果

Fig. 6　The recovery of bimodal aerosol PSDs at different velocities

表5 双峰气溶胶反演结果的性能指标

Table 5 The performance indices of the recovery of bimodal PSDs

Velocity/(m·s^{-1})	Method	PP/nm	E_{P0}	E_{F0}	Cond
0	Tik	180/740	0/0	0/0	2.41×10^{7}
0.50	Tik	130/720	0.277 8/0.027 0	0.009 5	3.10×10^{7}
	Pre-Tik	170/740	0.055 6/0	0.003 1	2.41×10^{7}
1.28	Tik	80/600	0.555 6/0.189 2	0.017 6	6.24×10^{7}
	Pre-Tik	200/690	0.111 1/0.067 6	0.010 8	2.41×10^{7}

4 结论

在流动气溶胶DLS测量中,被测颗粒的定向流动导致基于光强ACF构建的反演方程病态性增加,流速越快,方程的病态程度越高,表现为反演方程核矩阵的条件数增加。作为降低病态性常用方法的正则化反演方法,其在流动导致方程病态性增加时,不能完全消除流动导致的条件数增加问题。正则化方法在流动颗粒反演中的这种局限性,可通过条件预优改善。通过条件预优处理,以先验流速信息和延迟时间构建对角阵形式的条件预优矩阵,对病态方程进行乘法修正,可降低流速对反演方程病态性的加剧作用,从而降低流动气溶胶DLS测量时正则化反演方法对流速增加的敏感性。模拟与实测数据的反演结果表明,对于流动颗粒的DLS测量,采用结合条件预优的正则化反演,可以克服正则化方法在降低条件数过程中存在的局限性,改善PSD反演的性能指标,提高流动气溶胶DLS测量的准确性。

参考文献

[1] ISO 22412-2017, Particle size analysis-Dynamic Light Scattering (DLS)[S]. Geneva: International Organization for Standardization, 2017.

[2] PECORA R. Dynamic light scattering measurement of nanometer particles in liquids[J]. Journal of Nanoparticle Research, 2000, 2(2):123-131.

[3] GUO Xiaohui, CHEN Miao, LI Peng, et al. Particle size distribution inversion in dynamic light scattering by adaptive step-size non-negative least squares[J]. Optics Communications, 2022, 503: 127444.

[4] CHEN Mei, WANG Yanghong, LI Wei, et al. A dual-angle fiber dynamic light scattering system integrated with microfluidic chip for particle size measurement[J]. Optics & Laser Technology, 2022, 150: 107891.

[5] CHOWDHURY D P, SORENSEN C M, TAYLOR T W, et al. Application of photon correlation spectroscopy to flowing Brownian motion systems[J]. Applied Optics, 1984, 23(22): 4149-4154.

[6] TAYLOR T W, SORENSEN C M. Gaussian beam effects on the photon correlation spectrum from a flowing Brownian motion system[J]. Applied Optics, 1986, 25(14): 2421-2426.

[7] WEBER R, SCHWEIGER G. Photon correlation spectroscopy on flowing polydisperse fluid-particle systems: theory[J]. Applied Optics, 1998, 37(18): 4039-4050.

[8] WEBER R, SCHWEIGER G. Simultaneous in-situ measurement of local particle size, particle concentration, and velocity of aerosols[J]. Journal of Colloid and Interface Science, 1999, 210(1): 86-96.

[9] WANG H, SHEN J, WANG B, et al. Laser diode feedback interferometry in flowing Brownian motion system: a novel theory[J]. Applied Physics B, 2010, 101: 173-183.

[10] MU Tongtong, SHEN Jin, WANG Mengjie, et al. Particle size distribution measurement in a flowing aerosol using dynamic light scattering[J]. Measurement Science and Technology, 2021, 32(7): 075007.

[11] MU Tongtong, SHEN Jin, LI Xinqiang, et al. Velocity limitation in dynamic light scattering measurement for flowing aerosols[J]. Acta Optica Sinica, 2021,41(14):1429001.
牟彤彤, 申晋, 李鑫强, 等. 流动气溶胶动态光散射测量中的流速限制[J]. 光学学报, 2021, 41(14): 1429001.

[12] WINKLER J R. Tikhonov regularization in standard form for polynomial basis conversion[J]. Applied Mathematical Modelling, 1997, 21(10): 651-662.

[13] VARAH J M . A practical examination of some numerical methods for linear discrete ill-posed problems[J]. Siam Review, 1979, 21(1):100-111.

[14] TANG Longji, LI Wen, DENG Yangsheng. Some aspects for solving ill-posed equation in geophysics[J]. Acta Geophysica Sinica, 1995, 38(1): 105-114.
唐隆基, 李文, 邓阳生. 关于解地球物理中病态方程的若干问题[J]. 地球物理学报, 1995, 38(1): 105-114.

[15] TARANTOLA A. Inverse problem theory[M]. New York: Elsevier Science Publishing Company, 1987.

[16] THOMAS J C. Photon correlation spectroscopy: technique and instrumentation[C]. SPIE, 1991, 1430: 2-18.
[17] LIU Ling, CHEN Miao, QIU Jian, et al. Weighted bayesian inversion method in multi-angle dynamic light scattering measurements[J]. Chinese Journal of Computational Physics, 2019, 36(6): 673-681.
刘玲, 陈淼, 邱健, 等. 多角度动态光散射加权贝叶斯反演算法[J]. 计算物理, 2019, 36(6): 673-681.

Regularization Inversion with Preconditioner for Flowing Aerosols in Dynamic Light Scattering

HAN Jinzhuang, LI Xinqiang, SHEN Jin, WANG Baojun, LIU Wei, WANG Yajing
(*School of Electrical and Electronic Engineering*, *Shandong University of Technology*, *Zibo*, *Shandong* 255049, *China*)

Abstract: Dynamic Light Scattering (DLS) is a technique for submicron and nano Particles Size Distribution (PSD) measurement. With convenience and rapidity and no interference to the measured particle system, it is widely used in science and engineering. Generally, the DLS measurements are carried out with non-flowing samples in suspension, in which particles move only in the form of Brownian motion. In this situation, the fluctuations of scattered light of particles are only caused by the Brownian motion. Different from the DLS measurement of non-flowing particles in suspension, the translational motion of flowing particles leads to extra fluctuations of scattered light, making DLS measurement for flowing aerosols more difficult.

The key of flowing aerosol measurement is that the PSD is difficult to accurately recover, because the increase of velocity aggravates the ill-conditioned state of the inversion equation, which is manifested as the increase of the condition number of the kernel matrix. Regularization is a common equation. However, the effectiveness of regularization is restricted by increasing the velocities of flow particles. To solve this problem, in this paper, the inversion equation was preconditioned to reduce the condition number of the kernel matrix before the Tikhonov regularization was used, which significantly improved the accuracy of recovered PSDs for flowing particles.

To verify the effectiveness of the proposed method, the recovered PSDs of the 600 nm unimodal aerosols and 200 nm/700 nm bimodal aerosols with different velocities were simulated. The results show that the peak position error (E_P) and the distribution fitting error (E_F) of recovered PSDs become significant as the flowing velocity increases, which is represented that the particle size at the peak position is smaller than the true value and the distributions are wider than true distributions. Under the same flowing velocity, the recovered PSDs by preconditioned Tikhonov regularization (Pre-Tik) are closer to the true PSD than Tikhonov regularization (Tik). And the effect of preconditioning is increasingly obvious with the flow velocity increase. When the particle velocity is 2.0 m/s, the E_P and E_F of the PSD obtained by the Tik is 0.046 7 and 0.006 9 respectively, and by the Pre-Tik is 0.026 7 and 0.005 7 respectively. The simulated inversions of the 200 nm/700 nm bimodal PSDs show similar results in the particle size at both peaks position and the width of distribution, which results in the value of E_Ps and E_Fs rising. However, the performance indices of the inversion results of the two methods were quite different. When the flowing velocity is 2.0 m/s, the E_P and E_F of the PSD obtained by the Tik method are 0.660 0/0.274 3 and 0.012 1 respectively, while the E_P and E_F of the PSD obtained by the Pre-Tik method are 0.460 0/0.091 4 and 0.009 1 respectively. The accuracy of the recovered PSDs is improved by using the Pre-Tik method.

To further compare the performance of the Tik method and the Pre-Tik method, DLS experiments of flowing aerosols were carried out. The measured ACF data were obtained from a homemade DLS measurement platform for flowing aerosols. For unimodal flowing aerosols at 1.77 m/s, the E_P and E_F of PSDs reduced from 0.087 7 and 0.012 4 by using the Tik method to 0.052 6 and 0.008 6 by the Pre-Tik method. The recovery of the latter method is better than the former. For bimodal aerosol PSDs, the results are similar to unimodal aerosol PSDs. The E_Ps and E_Fs of the PSD recovered by the Pre-Tik method are smaller than those obtained by the Tik method, which agrees with the simulations.

The inversion results of simulated and experimental data show that the limitations of the regularization

method in DLS measurements of flowing particles can be broken through by preconditioning. In this paper, the preconditioner in the form of a diagonal matrix constructed with priori velocity and delay time can weaken the ill-condition state of the inversion equation and makes regularization less sensitive to velocities. Compared with the Tikhonov regularization, the preconditioned Tikhonov regularization can improve the inversion performance significantly for flowing aerosols in DLS measurement.

Key words: Dynamic light scattering; Aerosols; Inversion; Particle size measurement; Regularization; Preconditioner

OCIS Codes: 290.5820; 290.5850; 290.3200

Foundation item: Natural Science Foundation of Shandong Province (No. ZR2020MF124), Shandong University of Technology and Zibo City Integration Development Project (No. 2019ZBXC011)